Available online at www.sciencedirect.com

SCIENCE DIRECT®

Earth and Planetary Science Letters 230 (2005) 273–287

EPSL

www.elsevier.com/locate/epsl

Caldera formation by magma withdrawal from a reservoir beneath a volcanic edifice

V. Pinel[a,b,*], C. Jaupart[a]

[a]*Laboratoire de Dynamique des Système Géologiques, Institut de Physique du Globe de Paris, CNRS UMR 7579, 4 place Jussieu, 75252 Paris Cedex 05, France*
[b]*Laboratoire de Géophysique Interne et Tectonophysique, Université de Savoie, Le Bourget-du-Lac, France*

Received 23 April 2004; received in revised form 12 November 2004; accepted 16 November 2004
Available online 12 January 2005
Editor: V. Courtillot

Abstract

Caldera formation has been explained by magma withdrawal from a crustal reservoir, but little is known about the conditions that lead to the critical reservoir pressure for collapse. During an eruption, the reservoir pressure is constrained to lie within a finite range: it cannot exceed the threshold value for eruption, and cannot decrease below another threshold value such that feeder dykes get shut by the confining pressure, which stops the eruption. For caldera collapse to occur, the critical reservoir pressure for roof failure must therefore be within this operating range. We use an analytical elastic model to evaluate the changes of reservoir pressure that are required for failure of roof rocks above the reservoir with and without a volcanic edifice at Earth's surface. With no edifice at Earth's surface, faulting in the roof region can only occur in the initial phase of reservoir inflation and affects a very small part of the focal area. Such conditions do not allow caldera collapse. With a volcanic edifice, large tensile stresses develop in the roof region, whose magnitude increase as the reservoir deflates during an eruption. The edifice size must exceed a threshold value for failure of the roof region before the end of eruption. The largest tensile stresses are reached at Earth's surface, indicating that faulting starts there. Failure affects an area whose horizontal dimensions depend on edifice and chamber dimensions. For small and deep reservoirs, failure conditions cannot be achieved even if the edifice is very large. Quantitative predictions are consistent with observations on a number of volcanoes.
© 2004 Elsevier B.V. All rights reserved.

Keywords: caldera collapse; magmatic pressures; volcanic stress fields; volcano stability

* Corresponding author. LGIT-Université de Savoie, Campus Scientifique, 73376 Le Bourget du Lac, Cedex, France. Tel.: +33 4 79 75 86 51; fax: +33 4 79 75 94 06.
E-mail addresses: Virginie.Pinel@univ-savoie.fr (V. Pinel), jaupart@ipgp.jussieu.fr (C. Jaupart).

0012-821X/$ - see front matter © 2004 Elsevier B.V. All rights reserved.
doi:10.1016/j.epsl.2004.11.016

1. Introduction

Caldera formation is a rare and catastrophic event usually associated with the end of a volcanic cycle [1]. At Mount Pinatubo, Philippines, in 1991, and at Miyakejima Volcano, Japan, in 2000, the underlying magma reservoirs had been deflating for some time when calderas started to form [2,3]. This time sequence seems to be by far the most frequent one [4–6], and reservoir deflation has provided the framework for most papers on caldera collapse to date. Many studies have been aimed at the faulting pattern at Earth's surface and at the shape of the ensuing depression [7–16], but few have dealt with the full volcanic sequence leading to a caldera [17]. In the most common model, e.g., [12], the medium encasing the magma reservoir is initially in a state of lithostatic equilibrium with no edifice at the surface, and reservoir deflation leads to compressive stresses in the roof region. Because rocks are very strong in compression, this physical setup requires withdrawal to proceed to large reservoir underpressures. The possibility of sustaining an eruption for long enough has been questioned [18,19].

Here, we address two related issues: the magnitude of pressure changes in a volcanic magma reservoir and the stress field in roof rocks at failure. An eruption starts when the reservoir pressure increases and reaches the threshold for tensile failure of wall rocks [20]. This allows dyke formation, eruption and hence magma withdrawal from the reservoir. As a consequence, the reservoir pressure decreases. As long as the reservoir walls are in tension, feeder dykes can remain open. Once they are in compression, however, the dykes close, which stops the eruption. The reservoir pressure therefore cannot decrease below a certain value and one must assess whether it is sufficient for caldera collapse.

Few eruptions lead to failure of roof rocks above the reservoir, indicating that the necessary conditions are only met in special circumstances. The caldera forming eruption usually being at the end of a long sequence of "normal" eruptions, something must change in the volcanic system. One clue may be that most calderas form on preexisting edifice [21]. A volcanic edifice induces large stresses in the shallow crust and modifies the behaviour of a magma reservoir [22]. In this paper, we begin by examining whether or not failure conditions can be achieved in the roof region by realistic changes of reservoir pressure when there is no edifice. We then account for the presence of an edifice and reevaluate how stresses change during an eruption. We show that failure conditions can be reached once the edifice has grown to a certain size. Large tensile stresses are generated near Earth's surface, suggesting that calderas form due to faulting initiated there. We discuss the implications of the model and compare theoretical predictions to a number of observations. In Appendix A, we review model limitations and explain how our theoretical results, which have been obtained for a specific reservoir shape, may be used to evaluate other situations.

2. The elastic model

2.1. General considerations

The upper crust is characterized by Poisson's ratio ν and rigidity G. A volcanic edifice of radius R_e and height H_e rests above a cylindrical magma chamber of radius R_c and depth H_c. The reference state before loading is the lithostatic stress field with reservoir pressures set at lithostatic values. The theoretical model deals with perturbations from this reference state due to the edifice and to changes of reservoir pressure. In the reservoir, pressure is perturbed by an amount ΔP (Fig. 1), which is called an "overpressure" if it is positive and an "underpressure" if it is negative. For simplicity, the free surface above the reservoir is called "Earth's surface".

A convenient length-scale for this problem is the chamber depth H_c. Increasing ratio R_c/H_c from 0 to 1, we investigate the effects of increasingly large or increasingly shallow reservoirs. The slope of the edifice flanks, H_e/R_e, is set to 0.1 or 0.6, corresponding to a shield volcano with gentle slopes and to a stratovolcano with steep flanks, respectively. The theoretical model solves for elastic deformation in two dimensions (x,z), and details of the analytical calculations can be found in [22]. Here, we focus on deviatoric stresses at the traction-free boundaries (Fig. 1), the chamber walls ($\sigma_{\theta\theta}$) and Earth's surface (σ_{xx}), because they have the largest amplitudes.

2.2. Stresses at Earth's surface

Fig. 2 shows schematic horizontal profiles of normal horizontal stress σ_{xx} at the surface due to three different effects: reservoir overpressure, reservoir underpressure and loading by an edifice. The full solution is obtained by adding solutions for the edifice and reservoir effects. To achieve a simple understanding of the end result, we study each effect separately.

2.2.1. Overpressure in a reservoir with no edifice at Earth's surface

With no edifice, the solution may be found in the classical analysis of Jeffery [23]. An overpressured reservoir induces tension in the roof region near the axis and compression at large distances. At Earth's surface, horizontal stress σ_{xx} is given by (Fig. 3):

$$\text{at} \quad z = 0, \quad \sigma_{xx} = 4\Delta P R_c^2 \frac{\left(x^2 - H_c^2 + R_c^2\right)}{\left(x^2 + H_c^2 - R_c^2\right)^2}, \qquad (1)$$

where x is the horizontal distance. This may be greater than the reservoir overpressure ΔP, which illustrates

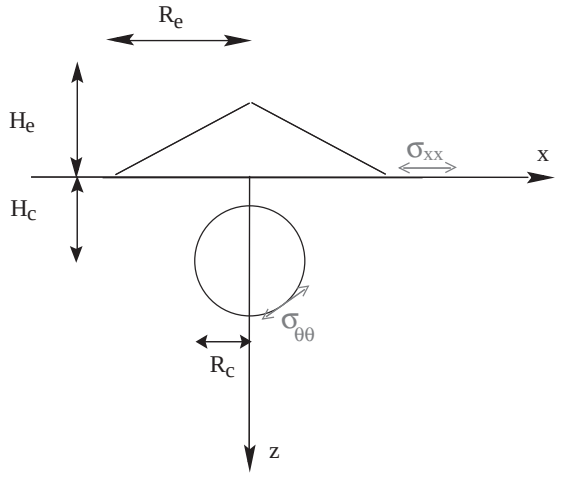

Fig. 1. Sketch of the model problem. A cylindrical reservoir of radius R_c lies at depth H_c, below an edifice of radius R_e and height H_e. Important stresses are those at the traction-free boundaries: σ_{xx} at Earth's surface and $\sigma_{\theta\theta}$ at the reservoir walls. The theoretical model solves for stresses and displacements due to the edifice load and to a change of reservoir pressure. The reference stress field is such that a neutrally buoyant magma reservoir lies in a lithostatic stress field.

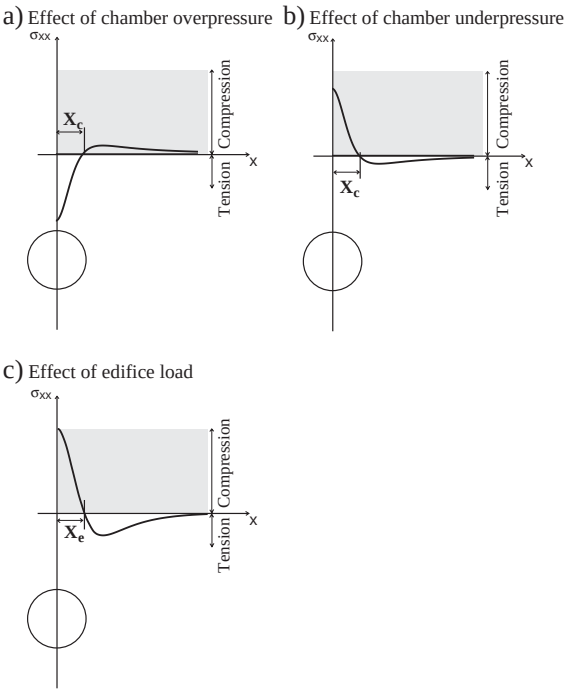

Fig. 2. Horizontal normal stresses at Earth's surface. (a) An overpressured chamber induces tension for $x<X_c$ and compression for $x>X_c$. (b) An underpressured chamber induces tension for $x>X_c$ and compression for $x<X_c$. (c) An edifice generates compression for $x<X_e$ and tension at larger distances. The general solution is obtained by summing the reservoir and edifice contributions.

how stresses may get amplified in a confined medium. σ_{xx} changes sign at $x = X_c = \sqrt{H_c^2 - R_c^2}$ and reaches a maximum in compression at $x = \sqrt{3}X_c$. Thus, Earth's surface is in tension for $0<x<X_c$ and in compression for $x>X_c$ (Fig. 2a). The maximum tensile stress is 8 times larger than the maximum compressive one, implying that Earth's surface, if it fails, does so first in tension.

For given depth H_c, increasing the reservoir size (increasing R_c) leads to an increasingly thinner roof and to concentrate tension in a small axial area, which acts to increase the magnitude of tensile stresses (Fig. 3). The maximum tension at Earth's surface is;

$$\sigma_{\max-\text{surf}} = -4\Delta P \frac{R_c^2}{H_c^2 - R_c^2}. \qquad (2)$$

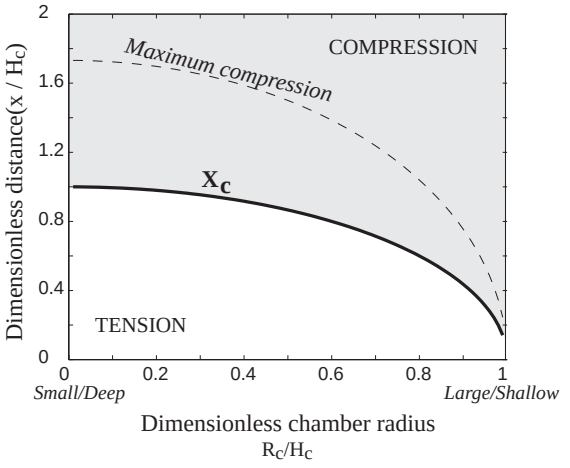

Fig. 3. Domains in compression and in tension at Earth's surface due to an overpressured reservoir with no edifice at Earth's surface as a function of dimensionless reservoir radius R_c/H_c. Earth's surface is in tension for $x<X_c$ and in compression for $x>X_c$. Maximum compression occurs at $x=\sqrt{3}X_c$.

In comparison, the maximum tensile hoop stress on the reservoir walls is [22]:

$$\sigma_{\max-\text{wall}} = -\Delta P\frac{H_c^2+R_c^2}{H_c^2-R_c^2}. \quad (3)$$

For $\frac{R_c}{H_c}>1/\sqrt{3}$, corresponding to shallow reservoirs, this is smaller than $\sigma_{\text{max-surf}}$. In this case, Earth's surface may fail before the reservoir walls and hence before eruption. More detailed considerations involving a failure criterion are developed later.

2.2.2. Underpressure in a reservoir with no edifice at Earth's surface

Results are exactly the previous ones in reverse (Fig. 2b). The chamber walls are in compression and tensile stresses are small everywhere. At the surface, the focal region is in compression and distal regions are in tension. For $\frac{R_c}{H_c}>1/\sqrt{3}$, the largest compressive stress is in fact reached at Earth's surface rather than at the chamber walls.

2.2.3. Loading by an edifice

We now consider stresses induced by an edifice at Earth's surface. The solution is obtained by requiring that the chamber pressure remains at its initial value when loading is applied [22]. The general problem of a change of reservoir pressure and loading by an edifice may then be obtained by adding this solution to the one above (i.e., for a reservoir with no edifice).

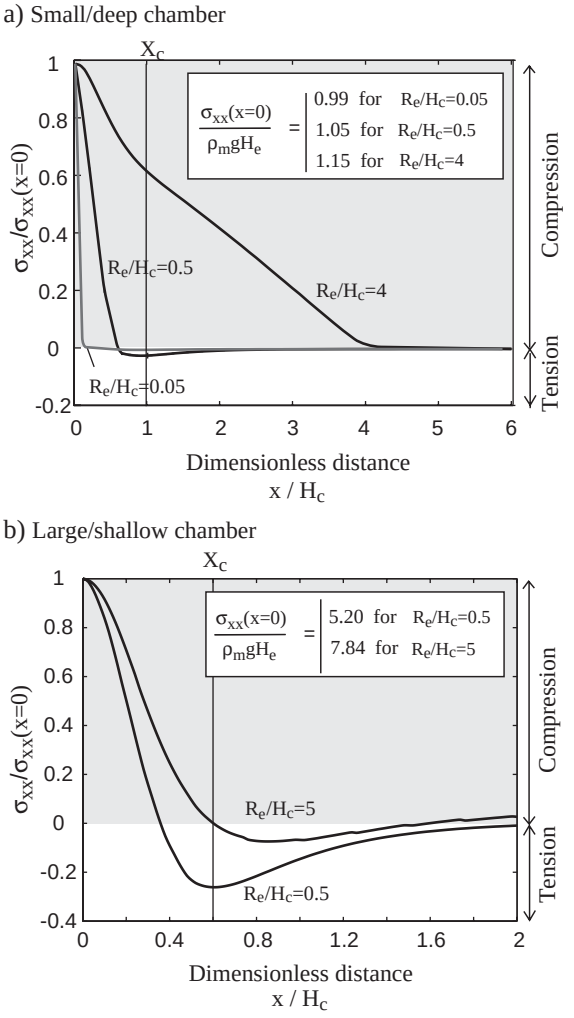

Fig. 4. Horizontal stress σ_{xx} at Earth's surface due to loading by a volcanic edifice as a function of distance. There is no reservoir overpressure. Stress values are scaled by the value at the origin σ_{xx} (x=0). Horizontal distance x is scaled to the chamber depth H_c. The vertical line stands for distance X_c, where changes of reservoir pressure generate no stress at Earth's surface (see Fig. 3). (a) Results for a small and deep magma chamber with dimensionless radius R_c/H_c=0.2. The inset shows values of σ_{xx} at x=0 as a function of edifice height H_e. (b) Results for a large and shallow magma chamber with dimensionless radius R_c/H_c=0.8. The inset shows values of σ_{xx} at x=0 as a function of edifice height H_e.

At Earth's surface, the edifice effect is the opposite of that of an overpressured chamber. At z=0, the horizontal stress σ_{xx} is compressive near the axis and becomes tensile at some distance (Fig. 2c). As above, it is useful to introduce the distance at which σ_{xx} changes sign, from compression to tension, which will be noted X_e. For a deep chamber (R_c/H_c=0.2), as the edifice radius increases, the solution tends to the limit case of a homogeneous half space, such that $\sigma_{xx}=\sigma_{zz}$ [24]. In this case, σ_{xx} at the surface decreases linearly from $\rho_m g H_e$ at x=0 to 0 at $x=R_e$ (Fig. 4a). For a shallow chamber (R_c/H_c=0.8), the effect of the edifice is enhanced and the compressive stress at the axis (at x=0) may be much larger than the applied load (Fig. 4b). The roof region behaves like a thin elastic plate and the zone of compression at Earth's surface is smaller than the edifice, i.e., $X_e<R_e$.

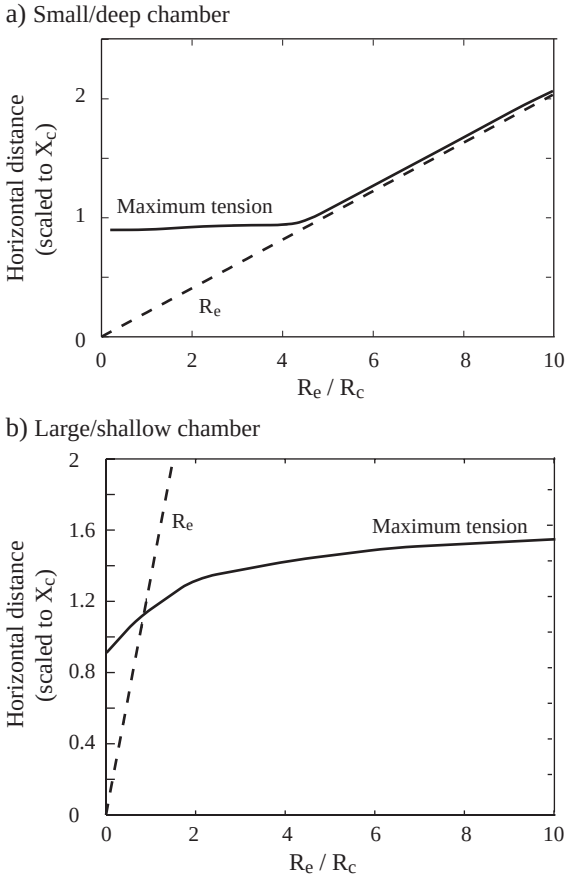

Fig. 5. Distance for maximum tension due to the edifice as a function of edifice radius. For ease of comparison, this distance is compared to the edifice radius (dashed line). All distances have been scaled to characteristic distance X_c, where stresses due to changes of chamber pressure change sign. Note that maximum tension can occur below the edifice, at distances smaller than R_e, or away from the edifice, at distances larger than R_e. (a) Small/deep chamber (R_c/H_c=0.2). (b) Large/shallow chamber (R_c/H_c=0.8).

Adding the effect of pressure changes in the chamber to this solution, which will be done later, leads to a complex stress field. We note that, at $x=X_c$, changes of chamber pressure induce zero stress at Earth's surface (Fig. 2), and hence the total stress reduces to the edifice contribution. At $x=X_c$, the edifice generates tension for $R_e \approx R_c$ and compression for $R_e \gg R_c$. In Fig. 5, we show the location of maximum tension induced by an edifice as a function of edifice radius R_e. Tension is largest at some distance of the edifice if the reservoir is deep and below the edifice if the reservoir is shallow.

These results emphasize that the presence of a reservoir may affect strongly the stress field generated by an edifice. Only when the reservoir is deep and the edifice is large does the reservoir influence become negligible. In that case, the maximum tension is generated at the edge of the edifice, at $x=R_e$ (Fig. 5a).

3. Stability of a volcanic system

Introducing a failure criterion, one may calculate which values of chamber pressure are required for roof breakdown. Rocks are much stronger in compression than in tension, and hence compressive failure requires very large deviatoric stresses. We have found that, in a volcanic system made of a reservoir and an overlying edifice, tensile stresses are large and exceed the strength of typical crustal rocks in many cases. In contrast, compressive stresses can be large only at the base of very big edifices over small parts of the focal area, and hence cannot be invoked for the formation of large calderas. In the following, we therefore focus on tensile failure.

We have found that, in the vast majority of cases, failure occurs first at Earth's surface, a result whose significance will be discussed later. For tensile failure at Earth's surface, we introduce two critical values depending on the reservoir pressure. In the initial phase of reservoir inflation, failure may occur when pressure increases above some critical value noted ΔP_1 (Fig. 6a). In this case, failure affects a small part of

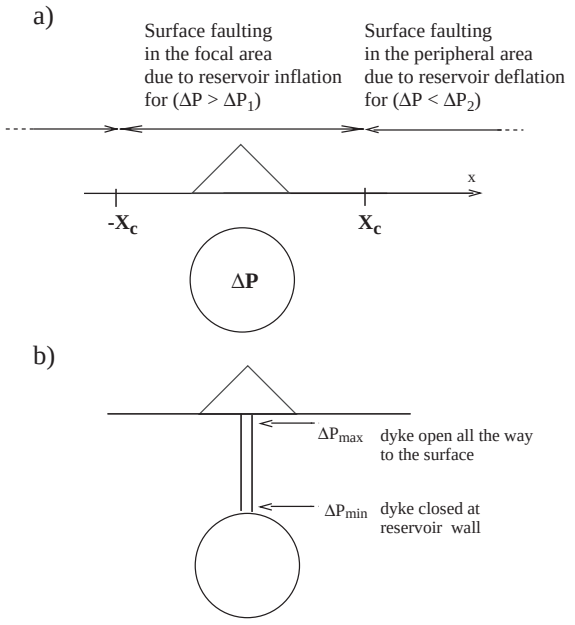

Fig. 6. (a) Schematic diagram showing where tensile failure may occur at Earth's surface depending on the magnitude of the pressure change in the reservoir. Reservoir overpressure ΔP_1 induces faulting in the focal area. There is a second, lower, critical pressure threshold ΔP_2 ($<\Delta P_1$) for which faulting occurs in distal regions, for $x>X_c$. (b) Bounds for pressure in a reservoir feeding an eruption. ΔP_{max} is the largest reservoir pressure, such that the reservoir walls are fractured and a feeder dyke remains open all the way to the surface. ΔP_{min} is the smallest reservoir pressure, such that feeder dykes close at the reservoir.

the focal area over a distance smaller than X_c. In the following phase of reservoir deflation, failure may occur when the reservoir pressure decreases below a second critical value, noted ΔP_2 (Fig. 6a). In that case, failure affects a much larger area over distances larger than X_c.

These results are not sufficient because they have been obtained without regard for two requirements: reservoir deflation can only occur if an eruption is underway, and reservoir deflation must proceed until the second critical pressure threshold ΔP_2. The onset of eruption defines the largest reservoir pressure, called ΔP_{max}. Conditions for the cessation of magma withdrawal define a lower bound for the reservoir pressure noted ΔP_{min}. These two pressures define the operating range for the reservoir pressure (Fig. 6b), and one must assess whether or not it encompasses the two critical pressure thresholds ΔP_1 and ΔP_2. Evaluating the conditions for roof failure therefore involves calculation of two sets of characteristic values for the chamber pressure: one set for tensile failure of the roof region (due to overpressure or underpressure), and a second set for the range of pressures that are allowed for a reservoir which feeds an eruption, i.e., a reservoir which remains connected to an open dyke or conduit.

3.1. Tensile failure

We assume that the same failure criterion applies to Earth's surface and the chamber walls. This criterion is such that the deviatoric stress exceeds some threshold value T_s, which is the tensile strength of country rock, as in [7,25] for example. Other failure criteria would not change the results significantly. For all numerical calculations, we take $T_s=2*10^7$ Pa.

At $z=0$, the perturbation stress tensor takes the following form:

$$\begin{pmatrix} \sigma_{xx} & 0 \\ 0 & \sigma_{zz} \end{pmatrix} \tag{4}$$

with σ_{zz} given by:

$$\sigma_{zz} = \frac{(R_e - x)}{R_e}\rho_m g H_e \quad \text{if} \quad x \le R_e$$

$$\sigma_{zz} = 0 \quad \text{if} \quad x > R_e. \tag{5}$$

In general, $\sigma_{xx}+\sigma_{zz}\neq 0$, and hence the deviatoric stress tensor is:

$$\begin{pmatrix} \frac{\sigma_{xx}-\sigma_{zz}}{2} & 0 \\ 0 & \frac{\sigma_{zz}-\sigma_{xx}}{2} \end{pmatrix} \tag{6}$$

The tensile failure criterion is thus:

$$\frac{\sigma_{xx}-\sigma_{zz}}{2} = -T_s. \tag{7}$$

The same criterion for failure at the chamber walls follows Pinel and Jaupart [22] and is such that:

$$\frac{\sigma_{\theta\theta}-\Delta P}{2} < -T_s. \tag{8}$$

3.2. An operating range for the chamber pressure

The chamber pressure is the sum of lithostatic pressure and an additional pressure ΔP which

increases due to magma replenishment or crystallisation [20]. The overpressure cannot increase indefinitely because it eventually acts to rupture the reservoirs walls. This triggers upward dyke propagation, but not necessarily eruption, because the dyke may stop before breaching Earth's surface. If the initial dyke stalls at depth, replenishment continues and the reservoir overpressure keeps on increasing until it is large enough to drive the dyke all the way to the surface. Once this is achieved, eruption ensues.

In summary, the largest chamber overpressure, noted $\Delta P_{\max}$, is such that eruption starts. This requires two conditions: (1) rupture of the reservoir walls and (2) dykes that are open at all depths. The first condition has already been specified. For the second condition, one must calculate the pressure distribution within a vertical magma column: for the dyke to be open, its internal magma pressure must be larger than the normal stress applied at its walls at all depths. In the present model, the density of magma in the reservoir is equal to that of encasing crustal rocks. The internal magma pressure within the dyke is the sum of the hydrostatic head and the viscous head loss. The limit case if that of volatile-free magma which stalls just below Earth's surface. In such a dyke, the internal magma overpressure is equal to ΔP at all depths and the normal stress applied at the vertical dyke walls is σ_{xx}. Thus, the condition that the dyke remains open all the way to Earth's surface is simply that:

$$\Delta P > \sigma_{xx}(0,0). \tag{9}$$

This defines $\Delta P_{\max}$. In practice, eruption would require a reservoir pressure slightly larger than this because of the additional effect of viscous head loss due to flow. For magmas with dissolved volatiles, the hydrostatic head in the dyke is smaller and hence the internal magma overpressure within the dyke may be larger than ΔP at shallow levels. In this case, an eruption can be sustained with reservoir pressures less than $\Delta P_{\max}$. Therefore, $\Delta P_{\max}$ is the largest pressure that can be achieved in the reservoir.

Once an eruption has started, one might envision that magma withdrawal is less efficient than replenishment, such that the reservoir keeps inflating. This is rarely observed in practice and we assume that eruption induces reservoir deflation. The reservoir pressure cannot decrease to any arbitrary value because large underpressures act to close off fractures at the chamber walls, and hence to snap shut feeder dykes for the eruption, which stops magma withdrawal. We call $\Delta P_{\min}$ the smallest reservoir pressure which may be achieved. Let us consider a feeder dyke at its inception point, i.e., at the edge of the reservoir. There, it may remain open as long as its internal magma pressure exceeds the normal stress applied at its walls. By continuity, the magma pressure within the dyke is equal to the chamber pressure. The normal stress at the dyke walls is equal to hoop stress $\sigma_{\theta\theta}$. Therefore, the minimum chamber pressure is such that:

$$\Delta P_{\min} = \sigma_{\theta\theta}. \tag{10}$$

Note that the eruption may stop before the reservoir pressure drops to $\Delta P_{\min}$. For example, if $\Delta P<0$, and if magma is volatile free, the reservoir pressure is smaller than the hydrostatic head between reservoir and Earth's surface and a surface eruption is impossible.

$\Delta P_{\max}$ is such that feeder dykes are open all the way to the surface. $\Delta P_{\min}$ is such that feeder dykes close at the reservoir walls. $\Delta P_{\max}$ and $\Delta P_{\min}$ are the upper and lower bounds for pressures in a reservoir feeding a surface eruption. For failure in the roof region, the critical values of chamber pressure ΔP_1 and ΔP_2 must be within this operating range. All these stresses must be calculated as a function of edifice size and chamber pressure.

3.3. Failure in the roof region

3.3.1. Without a volcanic edifice

This case allows compact analytical results. During the initial phase of reservoir inflation, the critical overpressure for failure at Earth's surface and the maximum chamber overpressure are:

$$\Delta P_1 = \frac{H_c^2 - R_c^2}{2R_c^2} T_s, \tag{11}$$

$$\Delta P_{\max} = \frac{H_c^2 - R_c^2}{H_c^2} T_s. \tag{12}$$

We note that $\Delta P_1 \le \Delta P_{\max}$ if $R_c/H_c \geq 1/\sqrt{2}$, corresponding to shallow reservoirs. In this case, failure of the roof region may occur before eruption. At Earth's surface, failure conditions are met at the axis, in practice over a very small area. The reservoir pressure is above the lithostatic value and hence can support the

weight of the roof region, which rules out caldera formation. We further discuss the force balance for the roof region in the discussion section below. With no caldera collapse, the reservoir may continue to inflate until its internal pressure reaches the threshold value for the onset of eruption.

If $R_c/H_c<1/\sqrt{2}, \Delta P_{max}<\Delta P_1$, such that eruption starts before failure at Earth's surface.

Once an eruption is underway, magma withdrawal lowers the reservoir pressure. In the deflation stage, the threshold reservoir pressure for tensile failure at Earth's surface is:

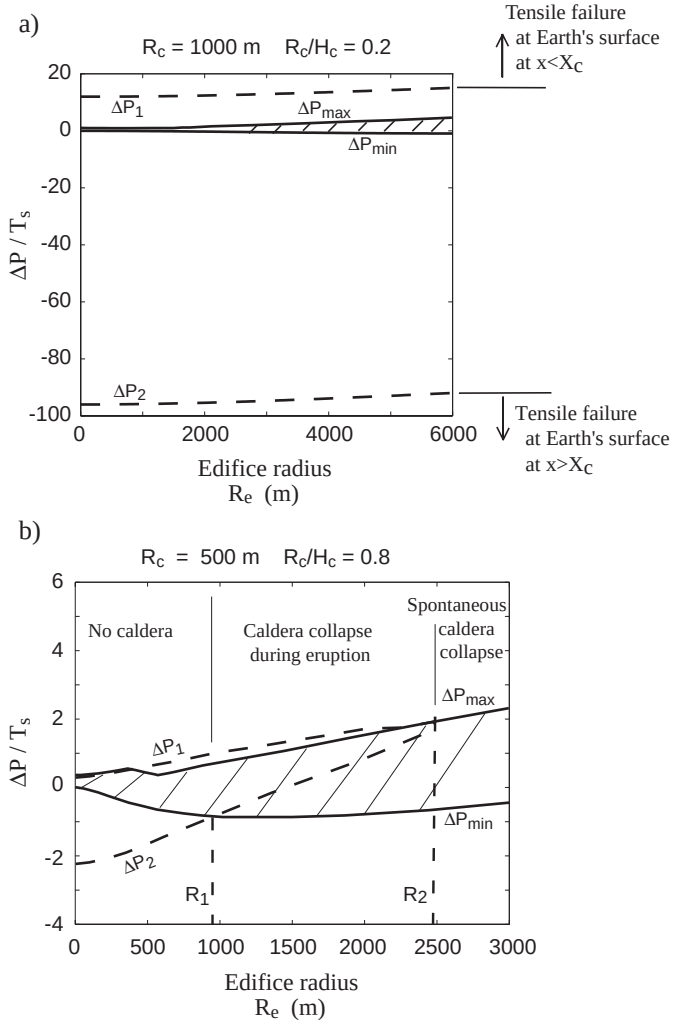

Fig. 7. Critical values of reservoir pressure for failure of the roof region as a function of edifice radius, ΔP_1 and ΔP_2. Also shown are the two extreme values of pressure for a reservoir which feeds an eruption, ΔP_{max} and ΔP_{min}. For caldera collapse, the critical values for failure must be within the "operating" range defined by ΔP_{max} and ΔP_{min}. Results are shown for a stratocone (with flank slopes H_c/R_c=0.6). (a) Case of a small and deep chamber (R_c/H_c=0.2), with R_c=1000 m. Given the operating range for the reservoir pressure (hatched area), no tensile failure can occur at Earth's surface. (b) Case of a large and shallow chamber (R_c/H_c=0.8), with R_c=500 m. Given the operating range for the reservoir pressure (hatched area), tensile failure is predicted at Earth's surface away from the axis if the edifice radius exceeds a critical threshold R_1. The lower curve for surface failure (ΔP_2) intersects the curve for the maximum chamber pressure (ΔP_{max}) for $R_c=R_2$. This defines the largest stable edifice size for this volcanic system.

$$\Delta P_2 = -4\frac{H_c^2 - R_c^2}{R_c^2} T_s. \quad (13)$$

Thus, $\Delta P_2<0$, showing that the reservoir must be underpressured for failure of the roof region. However, without an edifice, feeder dykes close off when $\Delta P=0$. Thus, in this case, $\Delta P_{min}=0$, implying that $\Delta P_2<\Delta P_{min}$ and hence that eruption stops before caldera collapse.

3.3.2. With a volcanic edifice

An edifice modifies the stress field in the roof region, with different results depending on reservoir depth. For a deep magma chamber, the critical pressure values for tensile failure at Earth's surface, ΔP_1 and ΔP_2, are well outside the operating pressure range for all values of the edifice radius (Fig. 7a). In this case, the edifice may keep growing without caldera formation and the volcanic system remains stable.

The situation is very different for shallow chambers. For $R_c/H_c=0.8$, for example, the four characteristic pressures, ΔP_1, ΔP_2, ΔP_{min} and ΔP_{max}, take similar values within a restricted range (Fig. 7b). Further, values for ΔP_1 and ΔP_{max} are very close to one another. We now describe results for edifices of increasing sizes. For small edifices, results are similar to those obtained above with no edifice. The roof region may fail over a small area during reservoir inflation, but caldera formation is unlikely for the same reasons as above: the reservoir pressure is sufficient to support the roof region and failure affects a very small part of the focal area. One eruption starts, the reservoir pressure decreases to ΔP_{min} without reaching the second failure threshold ΔP_2, i.e., the eruption stops before breakdown of the roof region. This behaviour obtains up to a critical edifice radius noted R_1 (Fig. 7b). For $R_e>R_1$, $\Delta P_2>\Delta P_{min}$ and hence reservoir deflation can proceed to the critical pressure threshold for roof breakdown. In this case, tensile failure occurs away from the axis and affects a large area at Earth's surface. Ultimately, when the edifice radius reaches a second critical value noted R_2, the roof cannot sustain the edifice load regardless of the reservoir pressure. This defines the largest edifice size for a stable volcanic system. Values of critical edifice radius R_2 are shown in Fig. 8a and b for two chamber sizes.

To summarize, if $R_e<R_1$, no caldera formation is expected for realistic reservoir pressures. If $R_1<R_e<R_2$, caldera formation may occur during reservoir deflation. Finally, if $R_e>R_2$, the roof region can be stable for no realistic values of the reservoir pressure. R_2 is therefore the maximum edifice radius for a working magma reservoir. In this limiting case, Earth's surface fails at distance $x=X_c$, which defines the final caldera size. For practical reasons, it is useful to compare it to the edifice radius which is readily measured in the field. For a shield volcano, for all reasonable values of chamber radius, the value of

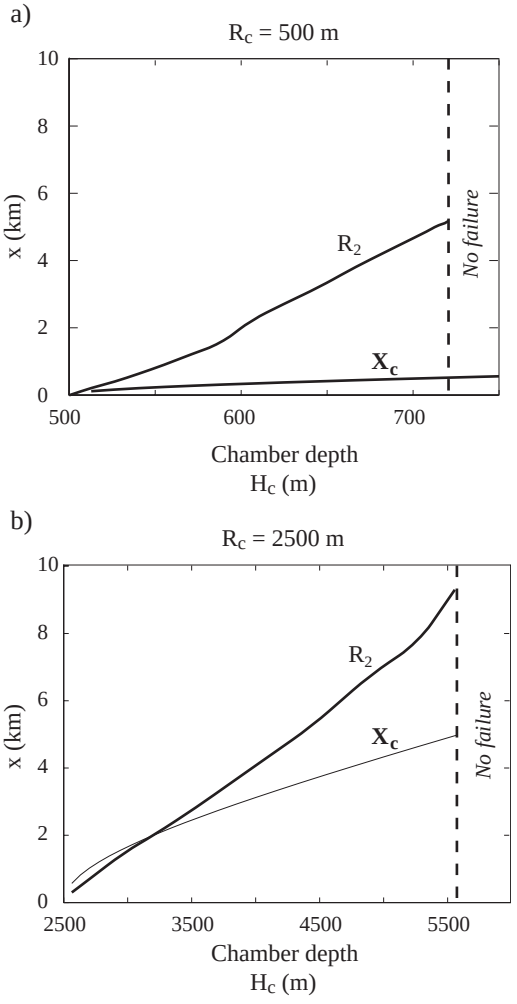

Fig. 8. Maximum stable edifice size R_2 (see Fig. 7) and distance of surface faults as a function of chamber depth. The edifice is a stratovolcano with slope $H_e/R_e=0.6$. If $R_e=R_2$, failure of Earth's surface occurs at distance $x=X_c$. (a) R_c=500 m: no surface failure is expected for H_c>750 m. (b) R_c=2500 m: no surface failure is expected for H_c>5550 m.

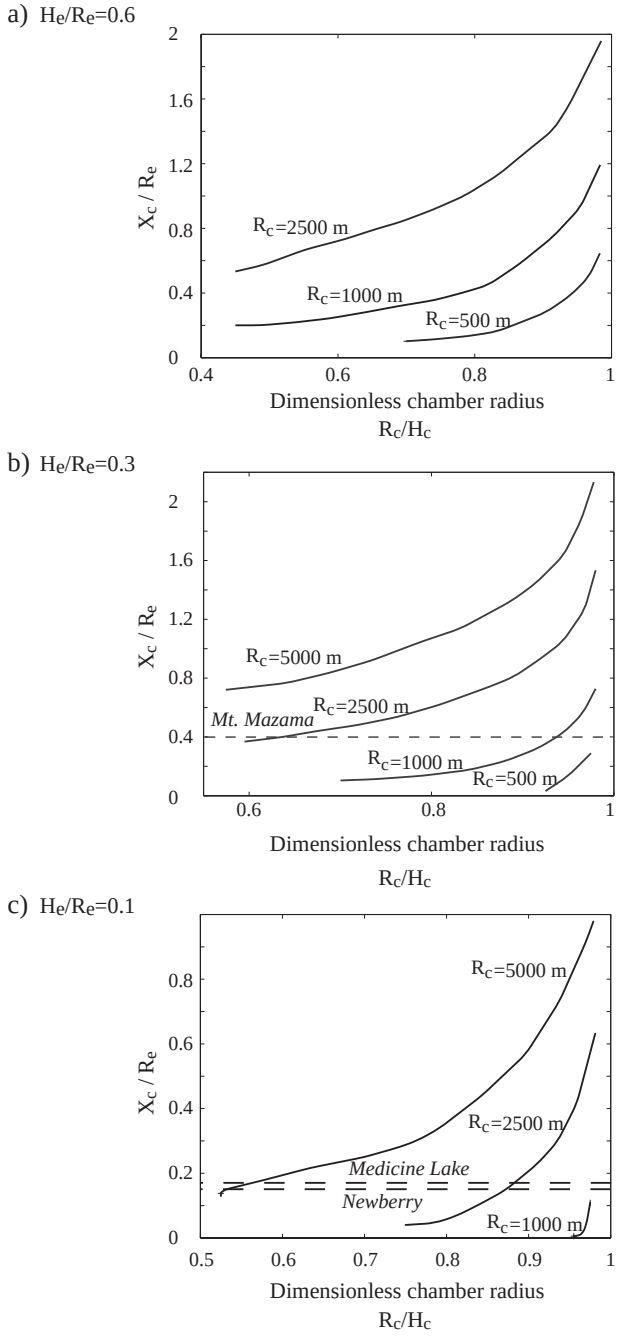

Fig. 9. Failure distance (scaled to the edifice radius) as a function of dimensionless chamber radius R_c/H_c. Results are shown for different edifice sizes. (a) Case of a statovolcano with slope H_e/R_e=0.6. (b) Case of a stratovolcano with Mount Mazama characteristics, i.e., flank slope H_e/R_e=0.3. The dashed line shows the caldera size for Mount Mazama. (c) Case of a shield volcano with slope H_e/R_e=0.1. Also shown are values for Medicine Lake and Newberry, two shield volcanoes in the Cascades range, Western North America.

ratio X_c/R_e is small (Fig. 9c), implying that the caldera is much smaller than the edifice. For a stratovolcano, this ratio is larger by a factor of about 2 (Fig. 9a). This suggests that measurements of caldera size and edifice size yield constraints on chamber size and depth.

4. Volcanological implications

4.1. Summary

Caldera collapse occurs after the onset of eruption, and hence involves two different kinds of failure. One is rupture of the reservoir walls, a prerequisite for eruption, which is achieved by reservoir inflation. The other kind of failure is collapse of the roof region, which is achieved by reservoir deflation. These two kinds of failure require two different stress fields in the roof region. We note that differences due to reservoir inflation and deflation are marked at shallow depths near Earth's surface and largest when there is a volcanic edifice. Without an edifice, failure of the roof region is restricted to the initial inflation stage, which cannot trigger caldera collapse, and reservoir deflation cannot proceed to the large magmatic underpressures required for roof breakdown. With an edifice, tensile failure of the roof region is possible during reservoir deflation. According to these calculations, faulting starts at Earth's surface. Gudmundsson [7] had already suggested such conditions, but the driving mechanism was different, involving flexure due to a large and deep reservoir below a small and shallow chamber.

As with all physical models of natural phenomena, these results are best suited to predict general trends in the observations, and should not be applied to specific cases without due attention for the various complications that may arise in practice, which are reviewed in Appendix A. The model explains why caldera collapse seldom occurs during reservoir inflation. It also explains why caldera collapse is a rare event and suggests that the triggering process is growth of a volcanic edifice. Another prediction is that caldera size should in general be smaller than reservoir size, which will be discussed below. We shall review the specific case of Mount Mazama and will discuss cases which seem inconsistent with the model predictions.

Once faulting occurs, the present model is no longer valid and we briefly discuss what happens in the next section.

4.2. The caldera collapse process

Once failure has occurred at Earth's surface, we may expect that fracturing extends downwards. Traction-free boundaries are subjected to large deviatoric stresses, which explains why fractures propagate from one such boundary to another, in our case from Earth's surface to the reservoir. Experiments by Mastin and Pollard [26] for the different case of a rising dyke illustrate what is likely to happen: fractures start at the surface and connect to the dyke tip. To study the fully developed faulting regime, the best strategy would probably be to use scaled laboratory experiments. With one exception [16], unfortunately, existing laboratory studies of caldera collapse have dealt with reservoir deflation starting from a state of lithostatic equilibrium, with no edifice at the surface.

Roche and Druitt [6] developed a model for "piston" calderas, such that the roof subsides as a coherent block bounded by ring faults. Using a vertical force balance on the block, with reservoir pressure applied at the base, friction on the ring faults and the weight of the block, they calculated the critical reservoir pressure below which the roof block can no longer be supported. For a cylindrical roof of radius R and height H, the magnitude of the reservoir underpressure, $|\Delta P_{(-)}|$, is proportional to the average friction on the ring faults, τ:

$$|\Delta P_{(-)}| = \tau \frac{2H}{R}. \quad (14)$$

Thus, failure over a small part of the focal area, which implies a very large value of H/R, may lead to a caldera only at very large reservoir underpressures. This shows why, for a shallow reservoir beneath a small edifice (or with no edifice at all), early faults generated in the inflation stage cannot be re-activated in the deflation stage. In the Roche and Druitt experiments, the block has almost the same size than the reservoir in horizontal cross-section. In our model, the size of the faulted area may be quite different and

this is discussed below. We note that, with an edifice at Earth's surface, the subsiding block is larger than the roof in the vertical dimension because it includes part of the edifice.

4.3. Caldera size

In our model, the size of the caldera is determined by faulting at Earth's surface, and may be quite different from the size of the underlying magma reservoir. Caldera formation is most likely for shallow reservoirs, in which case the caldera is smaller that the reservoir. This runs against the most common model of caldera formation, which relies on stoping of the reservoir roof [27]. In a typical experimental setup, a reservoir is filled in and then covered with brittle material (usually sand or flour), and is deflated to an arbitrary level chosen by the experimenter. By design, the reservoir is underpressured until the roof breaks down in compression. In this model, the roof fails first and a damage zone migrates upwards almost vertically, leading to a collapsed zone with the shape of the reservoir in horizontal cross-section. These predictions are difficult to test in the field because it is almost impossible to reconstruct the missing reservoir. To overcome this difficulty, Hildreth and Fierstein [28] studied the dimensions of a large number of calderas and plutons, and noted that, statistically, plutons are larger than calderas. They therefore concluded that, in general, calderas are smaller than their associated magma reservoirs. One might argue that plutons crystallize from the margins inwards and that the reservoir which is effectively liquid at the time of caldera collapse is smaller. However, observations on fossil intrusions, such as the Skaergaard complex of Greenland for example, demonstrate that the marginal zones are thin and account for a negligible fraction of the total horizontal cross-section [29]. This is well understood and explained by the inherently unstable nature of crystallizing boundary layers [30].

According to our calculations, the caldera accounts for a smaller fraction of the edifice in shield volcanoes than in stratovolcanoes (Fig. 9a and c). This is consistent with the field data. Wood [21] showed that, on average, the ratio of caldera size to edifice size is about 0.1 for shield volcanoes and 0.4 for stratovolcanoes.

4.4. Constraints on the size and depth of magma reservoirs

The present model predicts collapse within a specific range of chamber depth and size, which provides a simple test of its applicability. For example, Fig. 9c shows the ratio of caldera size (X_c being a lower limit for the failure distance) to edifice size for the Medicine Lake and Newberry shield volcanoes [31]. The predicted chamber sizes and depths lie within a realistic range of several kilometers.

We may test the model further in the specific example of Crater Lake caldera, which collapsed during the climatic eruption of Mount Mazama 6845 yr ago [32,33]. A 5 km diameter block subsided, so that we take this as an estimate of the structural caldera diameter (the topographic diameter being around 9 km [33]). The stratocone reached an elevation of about 3500 m [34], corresponding to an edifice height of about 1700 m. From the topographic map, we estimate that the edifice had a radius of 6 km and a slope H_e/R_e=0.3. It follows that ratio X_c/R_e had a value of about 0.4. In Fig. 9b, one may see that, for realistic values of dimensionless chamber size R_c/H_c, the chamber radius must be within a rather small range around 2500 m. On the one hand, larger chamber radii would imply very small values of R_c/H_c, and hence very deep chambers. A chamber radius of 5 km would not allow a value of 0.4 for X_c/R_e. On the other hand, smaller chamber radii would imply values of R_c/H_c close to 1, and hence a very shallow chamber. The erupted volume of about 50 km^3 [32] corresponds to a radius of 2.3 km, which is consistent with this argument. We note that, in this particular example, reservoir and caldera have similar radii. Using a chamber radius of 2.5 km, we find a chamber depth of about 4 km. Petrological estimates of magma pressure prior to eruption are available, but may be quite larger than the lithostatic pressure at the chamber depth, as explained by Pinel and Jaupart [22]. The pressure estimate by Bacon et al. [35] corresponds to lithostatic conditions at a depth of about 5 km. Taking into account the fact that this value must be regarded as an upper bound, our rough estimate of 4 km is quite reasonable.

Finally, the model may be applied to stable volcanic systems with no major calderas and puts limits on chamber size and depth. For a given edifice,

i.e., given values of R_e and H_e/R_e, one may exclude a whole range of values for R_c and H_c (Fig. 10). Mount Adams, for example, grew to a very large size without major caldera collapse. According to our model, this requires a small reservoir, which is consistent with petrological constraints: the rapid variation of erupted magma compositions indicates that there never was a major storage zone beneath this volcano [36].

4.5. The shape of the magma chamber

The present model cannot account for calderas over deep and small reservoirs. For example, the famous eruption of Mount Vesuvius in 79 AD led to a sizable caldera. The Vesuvius chamber is deeper than 6 km and the erupted volume was small (less than 5 km^3). Assuming that all the magma present in the reservoir was erupted, dimensionless number R_c/H_c is estimated to be less than 1/3 [27]. In this case, according to the present model, no caldera formation can occur if the chamber pressure remains within the "normal operating range". One possibility is that the Vesuvius chamber had a different shape. Seismic studies have tentatively outlined a sill-shaped magma reservoir at a depth of 8 km beneath the volcano [37]. The top of the chamber thus appears almost flat and extends over a distance larger than the edifice. In this case, the roof region behaves as an elastic plate which bends downwards as magma pressure is relieved. This behaviour is the same as that of a shallow cylindrical chamber [22] (Appendix A): bending stresses at the top of the reservoir enhance opening of feeder dykes and increase as the reservoir deflates. This is analogous to the "spontaneous collapse" regime of Fig. 7b. One problem with this explanation is that it does not account for the apparently stable growth of the edifice before the major caldera event. We note that Vesuvius collapsed very late in the eruption sequence, when the amount of magma erupted was about 80% of the total [27]. In a way, this may be considered consistent with the analysis developed here: for $R_c/Hc \approx 0.3$, the roof region can sustain large reservoir underpressures, implying that a large fraction of the chamber can be emptied without failure. The solution to this problem may be that Vesuvius involved two magmas with different densities [38]. Such conditions require a reevaluation of the criterion for the cessation of eruption (i.e., the equation for ΔP_{min}). A relevant discussion may be found in [18].

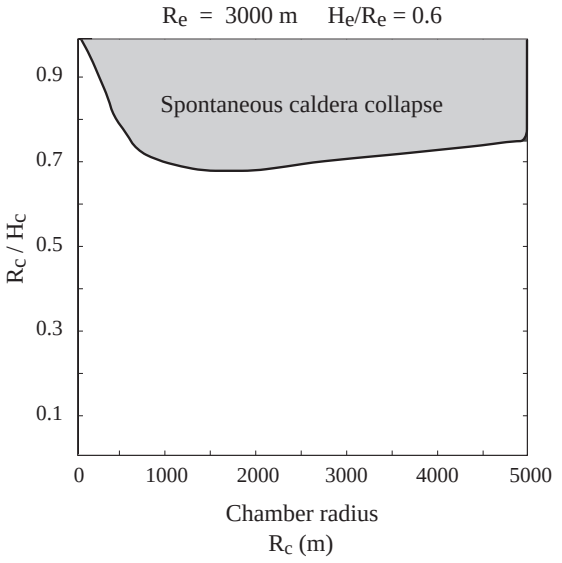

Fig. 10. Shows the sizes and depths of magma reservoirs (expressed in terms of variables R_c/H_c and R_c) which are in the spontaneous caldera collapse regime beneath a 3 km radius stratovolcano (Fig. 7). For these, by definition, R_2 is smaller than 3 km.

Some of the largest calderas were apparently not formed on pre-existing massive edifices [21]. It may be that all trace of the edifice has been destroyed, as very shallow magma chambers lead to calderas that are larger than the edifice. However, the sheer size of such calderas would require unrealistically large edifices. Mechanical and thermal conditions associated with the formation of enormous magma reservoirs probably play an important role and deserve study.

5. Conclusion

We have demonstrated that chamber pressures are constrained to lie within a finite operating range during an eruption, which limits the magnitude of stresses that can be generated in host rocks. One consequence is that stresses due a mature edifice at Earth's surface play a dominant role. With an edifice of sufficient size, caldera collapse can occur during chamber deflation, as the chamber pressure is no longer able to support the surface load. According to

this model, the relationship between caldera size and chamber size depends on chamber depth and edifice size. The ratio of caldera size to edifice size allows important constraints on the size and depth of the underlying magmatic reservoir. According to this analysis, the largest tensile stresses are generated at Earth's surface, suggesting that collapse propagates downwards.

Acknowledgements

We thank Tim Druitt and John Stix for their careful and detailed reviews of the manuscript.

Appendix A. Model assumptions

The mechanical model relies on two main assumptions: elastic behaviour of host rocks and a magma reservoir in the shape of a horizontal cylinder.

There is good field evidence for elastic (reversible) deformation on the short time-scale of an individual eruptive cycle. Thus, effects of reservoir pressure changes can be adequately described by an elastic model. Over the larger time-scales of edifice growth, viscous stress relaxation may be more important. Viscous relaxation time-scales have been estimated for the lithosphere as a whole, and are consistently larger than 5 Ma [39,40]. Such estimates are vertical averages and hence provide lower bounds for the cold upper crust. On a smaller scale, rocks encasing the magma reservoir get heated up, but viscous behaviour is limited to a thin high-temperature halo. One must note that stratovolcanoes are usually associated with positive free-air gravity anomalies, showing that their surface loads are not compensated [41].

The model solves for the behaviour of a cylindrical reservoir. For other shapes, one may rely on three basic principles. One is that a concentrated load acting on a thin roof induces bending, and hence tensile stresses, at the top of the reservoir. A second principle is that a large edifice generates compressive stresses over a large depth range. The third principle is that the hoop stress due to magmatic overpressure depends on the local wall curvature [42]. The chamber shape affects the magnitude of induced stresses. The most important parameter is the aspect ratio of the roof region, and one recovers the behaviour of a flat roof by considering a large reservoir.

Another set of assumptions involve material properties. For example, both the stress field around the reservoir and the pressure distribution within a feeder dyke would be affected if magma and host rocks have different densities. Such effects deserve an independent study.

References

[1] T.H. Druitt, L. Edwards, R.M. Mellors, D.M. Pyle, R.S.J. Sparks, M. Lanphere, M. Davies, B. Barreirio, Santorini volcano, Mem. Geol Soc. Lond. 19 (1999) 13–57.
[2] W.E. Scott, R.P. Hoblitt, R.C. Torres, S. Self, M.M.L. Martinez, T.J. Nillos, Pyroclastic flows of the June 15, 1991 climatic eruption of Mount Pinatubo, in: C.G. Newhall, R.S. Punongbayan (Eds.), Fire and Mud: Eruptions and Lahars of Mount Pinatubo, Philippines, University of Washington Press, 1996.
[3] N. Geshi, T. Shimano, T. Chiba, S. Nakada, Caldera collapse during the 2000 eruption of Miyakejima Volcano, Japan, Bull. Volcanol. 64 (2002) 55–68.
[4] P.W. Lipman, The roots of ash flow calderas in Western North America: windows into the tops of granitic batholiths, J. Geophys. Res. 89 (1984) 8801–8841.
[5] P.W. Lipman, Subsidence of ash-flow calderas: relation to caldera size and magma-chamber geometry, Bull. Volcanol. 59 (1997) 198–208.
[6] O. Roche, T.H. Druitt, Onset of caldera collapse during ignimbrite eruptions, Earth Planet. Sci. Lett. 191 (2001) 191–202.
[7] A. Gudmundsson, Formation of collapse calderas, Geology 16 (1988) 808–810.
[8] A. Gudmundsson, Formation and development of normal-fault calderas and the initiation of large explosive eruptions, Bull. Volcanol. 60 (1998) 160–170.
[9] H. Komuro, Y. Fujita, K. Kodama, Numerical and experimental models on the formation mechanism of collapse basins during Green Tuff orogenesis of Japan, Bull. Volcanol. 47 (1984) 649–666.
[10] H. Komuro, Experiments on cauldron formation: a polygonal cauldron and ring fractures, J. Volcanol. Geotherm. Res. 31 (1987) 139–149.
[11] J. Marti, G.J. Ablay, L.T. Redshaw, R.S.J. Sparks, Experimental studies of collapse calderas, J. Geol. Soc. (Lond.) 151 (1994) 919–929.
[12] O. Roche, T.H. Druitt, O. Merle, Experimental study of caldera formation, J. Geophys. Res. 105 (2000) 395–416.
[13] V. Acocella, F. Cifelli, R. Funiciello, Analogue models of collapse calderas and resurgent domes, J. Volcanol. Geotherm. Res. 104 (2000) 81–96.
[14] T.R. Walter, V.R. Troll, Formation of caldera periphery faults: an experimental study, Bull. Volcanol. 63 (2001) 191–203.

[15] B. Kennedy, J. Stix, J.W. Vallance, Y. Lavallée, M.-A. Longpré, Controls on caldera structure: results from analogue sandbox modeling, Geol. Soc. Amer. Bull. 116 (2004) 515–524.
[16] Y. Lavallée, J. Stix, B. Kennedy, M. Richer, M.-A. Longpré, Caldera subsidence in areas of variable topographic relief: results from analogue modeling, J. Volcanol. Geotherm. Res. 129 (2004) 219–236.
[17] T.H. Druitt, R.S.J. Sparks, On the formation of calderas during ignimbrite eruptions, Nature 310 (1984) 679–681.
[18] P. McLeod, The role of magma buoyancy in caldera-forming eruptions, Geophys. Res. Lett. 26 (1999) 2299–2302.
[19] J.E. Gardner, S. Tait, The caldera-forming eruption of Volcan Ceboruco, Mexico, Bull. Volcanol. 62 (2000) 20–33.
[20] S. Tait, C. Jaupart, S. Vergniolle, Pressure, gas content and eruption periodicity of a shallow, crystallising magma chamber, Earth Planet. Sci. Lett. 92 (1989) 107–123.
[21] C.A. Wood, Calderas: a planetary perspective, J. Geophys. Res. 89 (1984) 8391–8406.
[22] V. Pinel, C. Jaupart, Magma chamber behavior beneath a volcanic edifice, J. Geophys. Res. 108 (B2) (2003) 2072.
[23] G.B. Jeffery, Plane stress and strain in bipolar co-ordinates, Trans. R. Soc. Lond. 221 (1920) 265–293.
[24] I.N. Sneddon, Fourier transforms, Mc Graw-Hill, 1951, 542 pp.
[25] A. Gudmundsson, J. Marti, E. Turon, Stress fields generating ring faults in volcanoes, Geophys. Res. Lett. 24 (1997) 1559–1562.
[26] L.G. Mastin, D.D. Pollard, Surface deformation and shallow dike intrusion processes at Inyo Craters, Long Valley, California, J. Geophys. Res. 93 (1988) 13221–13235.
[27] O. Roche, Les mécanismes de formation des calderas: étude expérimentale et modélisation, Master's thesis, Université Blaise Pascal, (2000).
[28] W. Hildreth, J. Fierstein, Katmai volcanic cluster and the great eruption of 1912, GSA Bull. 112 (2000) 1594–1620.
[29] L. Wager, G. Brown, Layered igneous rocks, Oliver and Boyd, 1968, 588 pp.
[30] C. Jaupart, S. Tait, Dynamics of differentiation in magma reservoirs, J. Geophys. Res. 100 (1995) 17615–17636.
[31] R.J. Pike, G.D. Clow, Revised classification of terrestrial volcanoes and catalog of topographic dimensions, with new results on edifice volume, Open File Rep. 81-1038 (1981) 1–40.
[32] C.R. Bacon, Eruptive history of Mount Mazama and Crater Lake caldera, Cascade Range, USA, J. Volcanol. Geotherm. Res. 18 (1983) 57–115.
[33] K. Suzuki-Kamata, H. Kamata, C.R. Bacon, Evolution of the caldera-forming eruption at Crater Lake, Oregon, indicated by component analysis of lithic fragments, J. Geophys. Res. 98 (1993) 14059–14074.
[34] C.A. Wood, J. Kienle, Volcanoes of North America: United States and Canada, Cambridge University Press, 1990.
[35] C.R. Bacon, S. Newman, E. Stolper, Water, CO_2, Cl and F in melt inclusions in phenocrysts from three Holocene explosive eruptions, Crater Lake, Oregon, Am. Mineral. 77 (1992) 1021–1030.
[36] W. Hildreth, M.A. Lanphere, Potassium–argon geochronology of a basalt–andesite–dacite arc system: the Mount Adams volcanic field, Cascade Range of southern Washington, Geol. Soc. Amer. Bull. 106 (1994) 1413–1429.
[37] E. Auger, P. Gasparini, J. Virieux, A. Zollo, Seismic Evidence of an extended magmatic sill under Mt. Vesuvius, Science 294 (2001) 1510–1512.
[38] H. Sigurdsson, W. Cornell, S. Carey, Influence of magma withdrawal on compositional gradients during the AD 79 Vesuvius eruption, Nature 345 (1990) 519–521.
[39] C. Beaumont, Foreland basins, Geophys. J. R. Astron. Soc. 65 (1981) 291–329.
[40] J.A. Nunn, N.H. Sleep, Thermal contraction and flexure of intracratonal basins: a three-dimensional study of the Michigan basin, Geophys. J. R. Astron. Soc. 76 (1984) 587–635.
[41] D.L. Williams, C.A. Finn, Analysis of gravity data in volcanic terrain and gravity anomalies and subvolcanic intrusions in the Cascade Range, USA, and at other selected volcanoes, in: W.J. Hinze (Ed.), The Utility of Regional Gravity and Magnetic Anomaly Maps, Society of Exploration Geophysicists, 1985.
[42] E. Tsuchida, Y. Saito, I. Nakahara, M. Kodama, Stresses in a semi-infinite elastic body containing a prolate spheroidal cavity subjected to an axisymmetric pressure, Bull. JSME 25 (1982) 891–897.